ACS EARTH AND SPACE CHEMISTRY

http://pubs.acs.org/journal/aesccq

Article

Numerical Study of Mineral Nucleation and Growth on a Substrate

Fengchang Yang,* Ke Yuan, Andrew G. Stack, and Vitalii Starchenko*

Cite This: *ACS Earth Space Chem.* 2022, 6, 1655−1665

Read Online

ACCESS | Metrics & More | Article Recommendations

ABSTRACT: Nucleation and growth processes of minerals and other crystals can significantly affect one another due to the transport limitations and local depletion of reactive ions in the solution. Most numerical models and experimental measurements have typically focused on either growth or nucleation, but not both. In this work, we incorporate a heterogeneous nucleation process based on classical nucleation theory into a micro-continuum model that implements the Darcy−Brinkman−Stokes approach to study the interplay between nucleation and crystal growth on a substrate in diffusive systems. We demonstrate how the Damköhler number (reaction rate) and nucleation rate prefactor change the effective nucleation rate on a substrate. Higher surface growth rates deplete the solute concentration around the nuclei that appear initially on the substrate, creating islands that screen against further nucleation. The model predicts that measured nucleation rates may be affected by the history of crystal nucleation on the substrate. In the extreme case of high growth rates relative to diffusion, it predicts that the rate of subsequent nucleation is limited by reactant depletion. We introduce a nondimensional number α to represent the relation between surface propagation rate during growth and the heterogeneous nucleation rate. We show that it is important to control Damköhler number and α to achieve similar precipitation regimes at different reaction and nucleation rates. We suggest that the observed universality can guide the interpretation of experimental results on nucleation rates, since matching experiment can be achieved by tuning transport, reaction, and nucleation parameters simultaneously. In addition, we show how the bulk solution concentration affects the structure and topology of precipitation on a substrate.

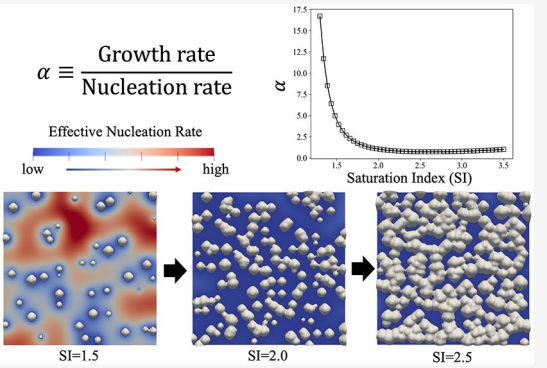

KEYWORDS: *crystal nucleation, crystal growth, mineral precipitation, pore-scale modeling, reactive transport modeling*

1. INTRODUCTION

Nucleation and growth of crystals from aqueous solutions are important to understand for natural phenomena such as biomineralization,[1] mineral precipitation,[2] and other fundamental crystallization phenomena.[3,4] In applied settings, understanding how to control mineral precipitation can be a strategy to remediate environmental contamination. It also can limit costs during oil−gas extraction, when scale formation in porous rock near wellbores significantly reduces permeability of the porous structure[5] and leads to a rapid decrease in production.[6] Industrially, the batch crystallization process can be significantly accelerated by enhancing nucleation[7] and is often used to separate and purify chemicals from solution in the pharmaceutical industry and other chemical manufacturing processes. Hence, the need to understand crystal nucleation and growth processes and their underlying mechanisms becomes crucial for the development of novel technologies.

Crystal nucleation is a complex process with poorly constrained mechanisms that are still debated.[8] Recently, molecular dynamics[9] and classical density functional theory[10] approaches were used to study the initial stages of crystal nucleation. For example, Dashtian et al.[9] used molecular dynamics to study nucleation of salt crystals in clay minerals and found nucleation happens in the interlayer of the clay particles initially filled with oversaturated brine. However, it is typically impractical to use these methods to model crystal formation distributions in larger systems due to computational restrictions, even for the most efficient implementations.

At larger scales, such as the macroscale, the crystal nucleation process has usually not been included in past simulations (they start with existing solid phase)[11,12] or incorporated into the overall precipitation process. Existing precipitation models use different techniques such as phase field,[13,14] volume of solid,[15,16] lattice Boltzmann,[17] level-set,[18] and others to track the change of solid phase. Examples of microscale precipitation models include Tartakovsky et al., who used smoothed particle hydrodynamics method to study

Special Issue: Hochella Honorary

Received: November 1, 2021
Revised: April 2, 2022
Accepted: May 19, 2022
Published: June 9, 2022

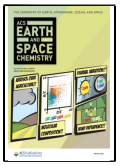

the reactive transport and mineral precipitation in fractured and porous materials.[19,20] Kang and colleagues studied various of dissolution and precipitation problems at pore scale using lattice Boltzmann method (LBM) models.[17,21,22] Modeling results based on level-set approach were used to fit the experimental observation of calcium carbonate precipitation in fractures.[18] Jones and Detwiler demonstrated the role of mineral heterogeneity could significantly affect the evolution of transport process in fractures. Yang et al. applied the Darcy−Brinkman−Stokes (DBS) model to model the precipitation of mineral within pore structure as well as crystal-face specific growth.[23] All these precipitation models advanced the knowledge of crystal mineral growth at larger scales; however, separating nucleation from crystal growth and then accounting for their interplay was not addressed explicitly.

Recently, a few studies started to capture nucleation and growth of crystals individually. Prasianakis and colleagues implemented the classical nucleation theory-based nucleation process and coupled it with LBM to model both the homogeneous and heterogeneous nucleation at pore scale in aqueous solutions.[24] They found that at a high saturation index (SI), homogeneous nucleation prevented the formation of barite through heterogeneous nucleation (epitaxially grown rim) at pore scale. Work by Starchenko[25] incorporates probabilistic nucleation into the pore-scale model based on the arbitrary Lagrangian-Eulerian approach. The nucleation was implemented on explicit interfaces of solid particles in reactive flow. It was shown by two-dimensional (2D) modeling that nucleation has a larger impact on the porosity of a precipitate at higher reaction rates. Additionally, nucleation promotes formation of irregularly shaped precipitates by enhancing instabilities in surface growth. Also, low nucleation rate reduces the impact of flow direction on the asymmetry of the formed precipitate around the particle. Deng et al. studied the effect of homogeneous nucleation on mineral precipitation by adding a correction to the reaction rate term and a precipitation band initiated by nucleation.[26] Through this method, they revised Archie's law, for effective diffusivity in a porous medium, to account for the clogging effect explicitly. In more recent work, Deng et al.[27] used a probabilistic nucleation with microcontinuum approach to precipitation to fit dissolution−precipitation experiments.

A recent experimental study reported rates of both heterogeneous nucleation and growth simultaneously.[28] Although these studies explore a combination of precipitation and nucleation, the question of how nucleation and growth processes influence each other at the microscale, if at all, remains open. Recent work of Yang and Steefel reported on conversion of forsterite to magnesite under high pCO_2 conditions combined with reactive transport modeling that included a heterogeneous nucleation process.[29] Fazeli et al.[30] introduced probabilistic nucleation by calculating random induction times. They used 2D LBM to explore various concentrations, growth rates, and flow rates.

Nucleation will be expected to be influenced by the reactant transport and reactivity as well. Therefore, pore-scale reactive transport modeling is a necessary tool to advance understanding of the interplay, if any, between crystal nucleation and growth processes. Particularly, it is not obvious whether nucleation always plays a crucial role in mineral precipitation or there are conditions at which the nucleation process can be neglected. In order to address these outstanding questions of the interplay between nucleation and growth, we coupled a microcontinuum simulation approach based on the DBS equation with classical nucleation theory due to its ability to model the phase change process.[31] In this work, we demonstrate that the transport of species and crystal growth play a role in the nucleation process on a flat substrate.

This manuscript starts with the details of the implementation of the nucleation process within the DBS model and the verification of the solver. After that, we demonstrate how the precipitate covers a flat substrate surface at different reaction and nucleation rate conditions. Further, we develop a dimensionless number, α, that reflects the competition between crystal growth and crystal nucleation processes. We show that this parameter describes the precipitation regime which can be reproduced at different values of measured nucleation and growth rates. Finally, we demonstrate the change in precipitation regime by varying bulk reactant concentration, which can be linked to α.

2. METHODS

To model the reactant transport and precipitation process in this work, we use the DBS approach developed in our previous study within the solver mpFoam.[23] In the current study, we implement a nucleation process and consider only diffusive transport from an infinite reservoir. Therefore, we solve the reaction−diffusion equation to model the transport of species:

$$\frac{\partial(1-\varepsilon_s)c}{\partial t} = \nabla\cdot(D_{\text{eff}}\nabla c) - \dot{R}_g - \dot{R}_n \tag{1}$$

where c is the concentration of reactive species, ε_s is the volume fraction of solid in a local cell, D_{eff} is the effective diffusion coefficient which relates to the bulk diffusion coefficient, D, as $D_{\text{eff}} = (1-\varepsilon_s)^2 D$, $\dot{R}_g$ is the reaction rate, and $\dot{R}_n$ is the source term related to nucleation rate.

We consider a binary precipitation reaction: $A + B \rightarrow AB$. Additionally, we consider diffusion of only a single reactive species due to the electroneutrality constraint at scales larger than the Debye length in the solution. The reaction rate was simplified as a first-order reaction:

$$\dot{R}_g = k a_v (c - c_{\text{sat}}) \tag{2}$$

where k is the reaction rate constant (m/s), a_v is the area density of the liquid−solid phase interface within a computational cell (m^2/m^3), c is the concentration of species, and c_{sat} is the saturation concentration for species (mol/m^3).

To implement the mineral nucleation process as a module in the mpFoam solver, we used classical nucleation theory for heterogeneous nucleation.[32,33] The nucleation rate was determined by the following equation:

$$J = A\exp\left(\frac{-\Delta G^*}{k_B T}\right) \tag{3}$$

$$\Delta G^* = \frac{16\pi\gamma^3 V_{\text{mol}}^2}{3(2.303\text{SI}\times k_B T)^2} \tag{4}$$

where J is the nucleation rate ($nuclei/m^2/s$), γ is the surface free energy in ($mJ/\mu m^2$), V_{mol} is the molar volume of the solid phase (m^3/mol), SI is the saturation index of the solution (e.g., for barite, $\text{SI} = \log(a_{Ba}a_{SO_4}/K_{sp})$, where $K_{sp} = a_{Ba}a_{SO_4}$ at equilibrium), k_B is the Boltzmann constant, T is the temperature of the solution, and A is a prefactor accounting for collision frequency of solution ions with each other and the

https://doi.org/10.1021/acsearthspacechem.1c00376
ACS Earth Space Chem. 2022, 6, 1655−1665

substrate (nuclei/m^2/s). While both the prefactor, A, and the interfacial energy, γ, control the nucleation rate, here we vary only the prefactor and keep the interfacial energy fixed. This is simply a numerical convenience, in that nucleation rate scales linearly with A and superlinearly with γ (since it is raised to the third power inside of an exponential), so the sensitivity of the model to nucleation rate is more easily probed by varying the prefactor.

The locally averaged probability of mineral nucleation for a computational volume cell, ϕ_{loc}, was calculated by the following relation:

$$\phi_{loc} = J_{loc} \cdot A_{c,s} \cdot t_{unit} \quad (5)$$

where J_{loc} is the local nucleation rate (which depends on the local concentration of reactant in ϕ_{loc}), $A_{c,s}$ is the surface area of the substrate within the volume cell, and t_{unit} is the time period. The probability function only applies for small enough $A_{c,s}$ to prevent multiple nucleation events in the same computational cell at same time. We consider that nucleation happens only on the substrate surface. Neither homogeneous nucleation or heterogeneous nucleation on other growing crystals are considered. Once a nucleus appears in the cell, the growth process dominates the increase in volume fraction of the solid in the cell. In the past, studies have shown that such phenomenon could lead to overlap of crystals at high nucleation densities.[34] Therefore, this study is focused on sparse nucleation on a smooth substrate, and secondary nucleation events in the same cell are not considered. To calculate ϕ_{loc} and determine whether a nucleation event occurs, a random number generator from the standard C++ library was used. The nucleation probability was calculated for each computational cell on the substrate at the beginning of each time period, t_{unit}. In this study, we set it to be t_{unit} = 1 s. Once a computational cell was selected for nucleation, a small part of the species was assumed to convert from liquid phase to solid phase (solid volume fraction $VOF_s = 1 \times 10^{-6}$). Assuming spherical nuclei in most of our simulations, this volume fraction corresponds to the initial nuclei radius of 6.2 nm, which determines the nucleation source term $\dot{R}_n$ in eq 1.

To characterize the relation between nucleation time scale, defined by the nucleation rate, and the reaction time scale (correspondingly defined by reaction rate), we introduce a dimensionless number that is the ratio between crystal surface growth rate ($\dot{r}$) and nucleation rate (J):

$$\alpha = \frac{\dot{r} N_A}{J\beta} \quad (6)$$

and

$$\dot{r} = k(c - c_{sat}) \quad (7)$$

where k is the reaction rate constant in units of m/s, N_A is Avogadro's number, and β is a dimensionless constant 10^{12} to reduce the order of α close to ~O(1). The latter term (β) is introduced for convenience in representing the results. It does not imply that the nucleation rate is smaller than reaction rate.

Figure 1 shows the schematics of the simulation domain. The dimensions of the simulation domain ($L \times L \times H$) were set to 100 μm × 100 × μm × 50 μm. The top boundary of the simulation domain was set as the bulk concentration c_b, which represents the large reservoir of solution at constant chemical potential. To mimic a large substrate, the four side boundaries of the simulation box were set as the symmetry boundary

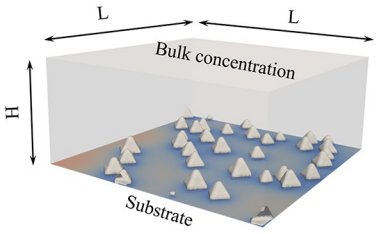

Figure 1. Schematics of the simulation domain. Bottom plane represents a solid substrate. Top plane corresponds to a Dirichlet boundary condition which specifies fixed value (bulk concentration, c_b) for the concentration field, thus mimicking a constant chemical potential experiment at fixed SI.

condition which enforces a symmetry constraint on concentration field. The bottom plane represents a solid substrate, on which the boundary for the concentration field was set to zeroGradient boundary condition. It applies a normal gradient of a field to be zero. At initial time, the concentration of solution within the simulation domain was set as the bulk concentration c_b. The simulation domain was discretized into a Cartesian grid of computational cells 1 μm in length, which is small enough to obtain to prevent multiple nucleation events in the same computational cell at same time (see verification case in Figure 2b). One artifact that this numerical implementation introduces is the shape of the nuclei, which is pyramidal (Figure 1). This problem becomes significant at later stages of the growth because it determines the end shape of total precipitate (especially at fast grow rates). However, the priority for this study is to focus on the relative rates of incipient nucleation and early growth of the nuclei. Thus, for the purposes of this manuscript, we neglect this artifact.

In this study, we focus on investigating the interplay between mineral nucleation, growth, and transport of reactive species. Therefore, we conduct a parametric study, in which a set of parameters was chosen to be close to a real mineral, specifically, barite. Barite itself is somewhat common, but also can be thought of as a representative of a group of sparingly soluble, ionically bonded minerals.[35] However, more detailed studies on different types of specific crystals and substrates could be done in the future.

The molecular diffusion coefficient was set to 1.0×10^{-9} m^2/s, the solid-phase molar mass M_v = 200 g/mol, solution concentration SI = 2.1 with solubility product constant $pK_{sp} = -\log_{10} K_{sp}$ = 10, c_{sat} = 0.01 mol/m^3, surface energy γ = 33 mJ/m^2, molar volume $V_{mol} = 5 \times 10^{-5}$ m^3/mol.

To analyze the effect of reactant depletion on the nucleation rate on the substrate, we define the scaled nucleation rate as $J^* = \frac{J}{J_b}$, where J_b is the nucleation rate at reactant concentration that corresponds to the bulk-like solution concentration. Hence, J^* has a range from 0 to 1 depending on the local concentration near the substrate.

The tolerance for the concentration field in the numerical solver used for eq 1 was set to 1×10^{-8}. A mesh sensitivity study was performed to ensure the precipitation process was independent of the chosen mesh size. The solver mpFoam and the nucleation module were implemented using the open-source CFD package OpenFOAM.[36] The Crank−Nicolson method was used for the temporal discretization. For the spatial discretization the Gauss linear method implemented in OpenFOAM package was selected. The details of the numerical method can be found in the User Guide of

https://doi.org/10.1021/acsearthspacechem.1c00376
ACS Earth Space Chem. 2022, 6, 1655−1665

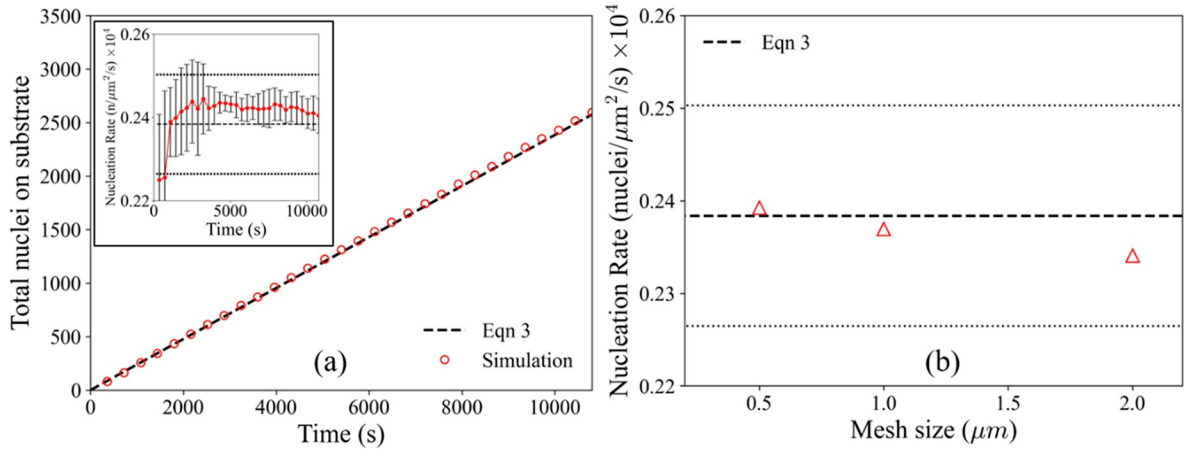

Figure 2. (a) Verification of the mineral nucleation process: total number of nuclei on substrate versus time. Inset shows the nucleation rate derived from the time dependence of the total number of nuclei. (b) Mesh size analysis: value of nucleation rate versus the cell size. Dashed line represents eq 3, and dotted lines show 5% deviation.

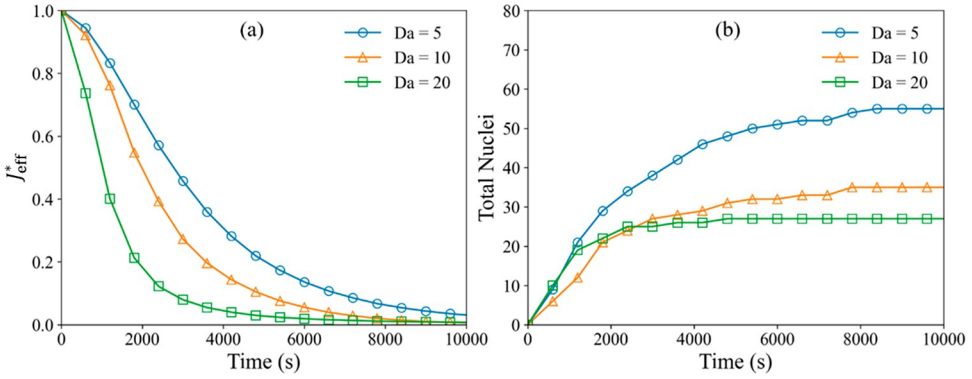

Figure 3. (a) Effective nucleation rate J^*_{eff} on a substrate as a function of time at different *Da*. (b) Total nuclei formed on a substrate as a function of time at different *Da*.

OpenFOAM. To perform the simulations, we utilized the CADES cluster at Oak Ridge National Laboratory and NERSC Cori supercomputer at Lawrence Berkeley National Laboratory.

3. MODEL VERIFICATION

To verify the implementation of nucleation in the mpFoam solver, the growth rate was set to zero and nucleation did not convert solute species to the solid phase. In such a way, we effectively separate nucleation from diffusion and reaction and remove the effect of reactant depletion near the surface. The bulk solution was set to the concentration c_b = 0.112 mol/m^3 (0.112 mM), which corresponds to a supersaturation SI = 2.1 for a K_{sp} of 10^{-10} (e.g., barite). The parameters for nucleation used in eq 3: molar volume $V_{mol} = 5 \times 10^{-5}$ m^3/mol, $A = 2 \times 10^8$ nuclei/m^2/s, γ = 33 mJ/m^2, and room temperature T = 298 K. Values of A and γ are from ref 28. In practice, measured values of γ for heterogeneous nucleation of sparingly soluble salts tend to range from 32 to 38 mJ/m^2 (see e.g., ref 37). Deviations far from this range tend to result in either no nucleation observed over the time scale of a typical experiment, or it occurs too quickly to resolve.

Figure 2a shows the comparison between the rate of nucleation and the analytical value according to eq 3 using fit parameters from barite formation on glass.[26] In the simulations (five simulation results averaged), we counted the number of nuclei that appear on the surface and calculated the total rate as a number of nuclei per time (insert of Figure 2a). It corresponds to the nucleation rate over the total surface of the substrate. The results of nucleation simulation (both nucleation rate and total nuclei on substrate) matched within the standard deviation (<3%) from the rate set by the parameters. The transport and phase change processes had been verified in our previous work ref 23. The results of a mesh size sensitivity analysis are shown in Figure 2b. At different mesh sizes, the nucleation rate was within 3% of deviation from eq 3. Considering both the accuracy and computational expenses, we chose the cell size as 1 μm for this study.

4. RESULTS AND DISCUSSION

4.1. Effect of Damköhler Number. To understand how the growth of existing mineral crystals affects the nucleation of new crystals on the substrate, we fixed diffusion and nucleation rates in the system and changed the reaction rate. The effective way of characterizing the relationship between reaction rate and transport is the dimensionless Damköhler number ($Da = \frac{kH}{D}$). The characteristic length scale H of the simulation system is 50 μm (height of the simulation domain), and the diffusion coefficient of solid species in solution is fixed. Hence, by tuning the reaction rate constant, k, we can change the Damköhler number. The prefactor A for nucleation was set as a fixed value, 2×10^7 nuclei/m^2/s. In first set of simulations,

https://doi.org/10.1021/acsearthspacechem.1c00376
ACS Earth Space Chem. 2022, 6, 1655−1665

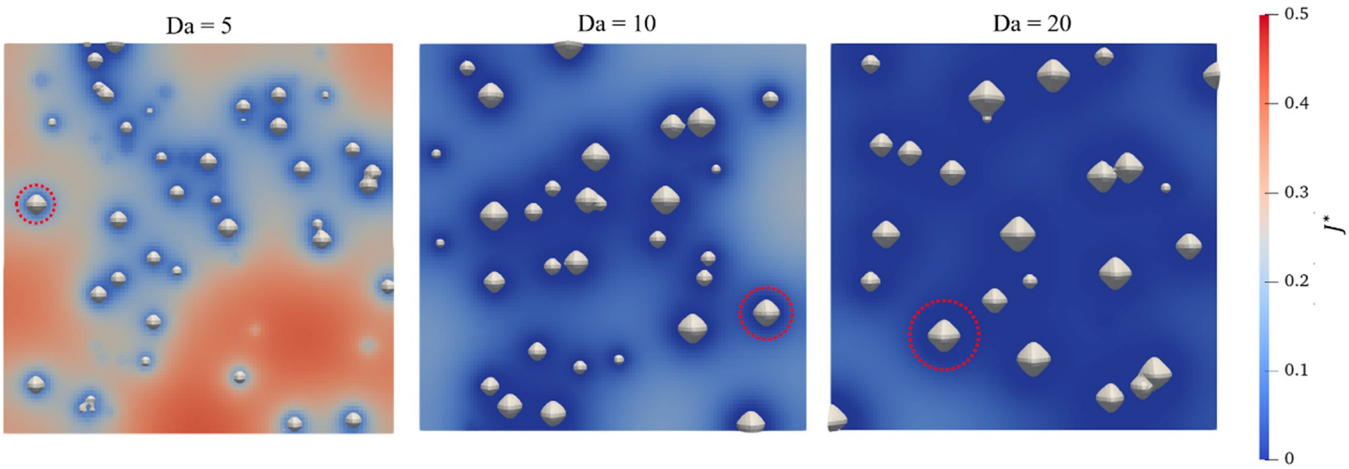

Figure 4. Scaled nucleation rate, J^*, for different *Da* numbers at 5000 s (gray area: solid phase). The color map shows the effective local nucleation rate, where blue areas denote that nucleation is suppressed relative to the pristine substrate. Red corresponds to the areas where the nucleation rate is still relatively high. Nucleation is suppressed by depletion zones surrounding growing nuclei, and the extent of the suppression is larger at higher Damköhler numbers. The red circles indicate the size of the depletion zone surrounding growing crystals.

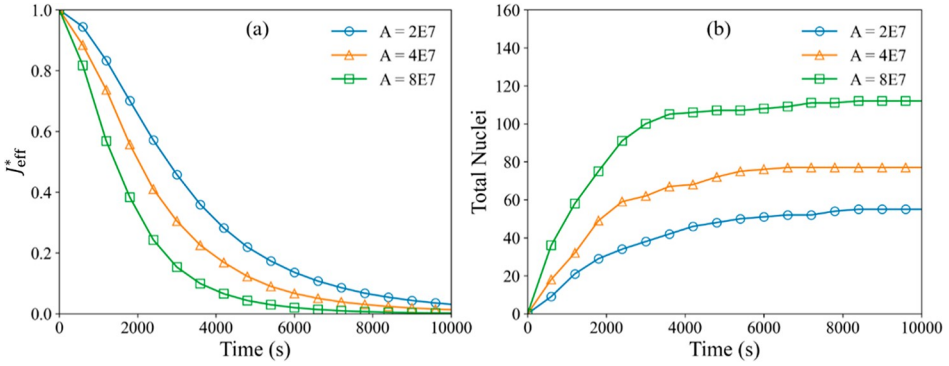

Figure 5. (a) Effective nucleation rate J^*_{eff} as a function of time for different nucleation prefactor *A*. (b) Total nuclei formed on substrate as a function of time for different nucleation prefactor *A*.

the Damköhler number was set to 5, 10, and 20 to observe its effect on the nucleation process. This range mimics some real mineral applications for the same system (e.g., barite: $Da \sim 7.5$ was used in ref 38, but contrasts with ref 28 where the *Da* was smaller).

Figure 3 shows the result of the simulations for different *Da* numbers. We calculate the effective nucleation rate, J^*_{eff}, at the substrate by averaging local J^* over the substrate area not covered by the solid phase. We only include the surface area where new crystals can be nucleated. In general, J^*_{eff} gradually decreases as a function of time (Figure 3a). Eventually, it drops to near zero, and no new crystals nucleate on the substrate surface (Figure 3b). The consumption of species by the growth of crystals reduces the local concentration near the substrate surface and subsequently leads to the drop of local nucleation rate *J*. It is demonstrated in Figure 4, which shows simulation snapshots of the distribution of nuclei and J^* on the substrate for different *Da* numbers. The snapshots are taken at $t = 5000$ s. The growth of the crystals reduces the local nucleation rate in their vicinity by creating diffusion gradients in the surrounding solution. The red circles around the growing crystals in Figure 4 indicate these depleted areas with lower local nucleation rates. Eventually, the substrate is screened from subsequent nucleation altogether. The growing crystals consume significant portions of the reactant before it can reach the substrate; therefore, the nucleation on the substrate becomes suppressed because the local saturation index has fallen enough such that nucleation is no longer probable.

As the reaction rate and the *Da* number increase, the nucleation on the surface decreases more rapidly (Figure 3a). Figure 3b shows the total number of nuclei on the substrate. Once the effective nucleation rate has dropped to zero, no new nuclei appear on the substrate and curves in Figure 3b plateau. Although the rate of nuclei number increase is the same for different *Da*, the maximum number of nuclei decreases as the *Da* increases. This observation reflects the zoning effect of the existing crystals, as it is shown in Figure 4. As the *Da* number increases, the consumption of solute species by crystal growth increases significantly, while the diffusion rate from the bulk only increases moderately due to the larger concentration gradient. Hence, each existing crystal creates a larger depletion zone (red circle in Figure 4) of mineral species as the *Da* number increase. The zoning effect at high growth rates suppresses the nucleation on the substrate and sequentially leads to lower nuclei density.

4.2. Effect of Nucleation Rate. In this section, the effect of changing the nucleation rate was examined by tuning the prefactor *A*, while the reaction rate and diffusion constant were fixed ($k = 1.0 \times 10^{-4}$ m/s and $D = 1.0 \times 10^{-9}$ m^2/s). Figure 5 shows the averaged J^* and total amount of nuclei as a function of time for different prefactor *A*. Similar to the trend observed in the previous section, the J^*_{eff} on the substrate decreases as a

https://doi.org/10.1021/acsearthspacechem.1c00376
ACS Earth Space Chem. 2022, 6, 1655−1665

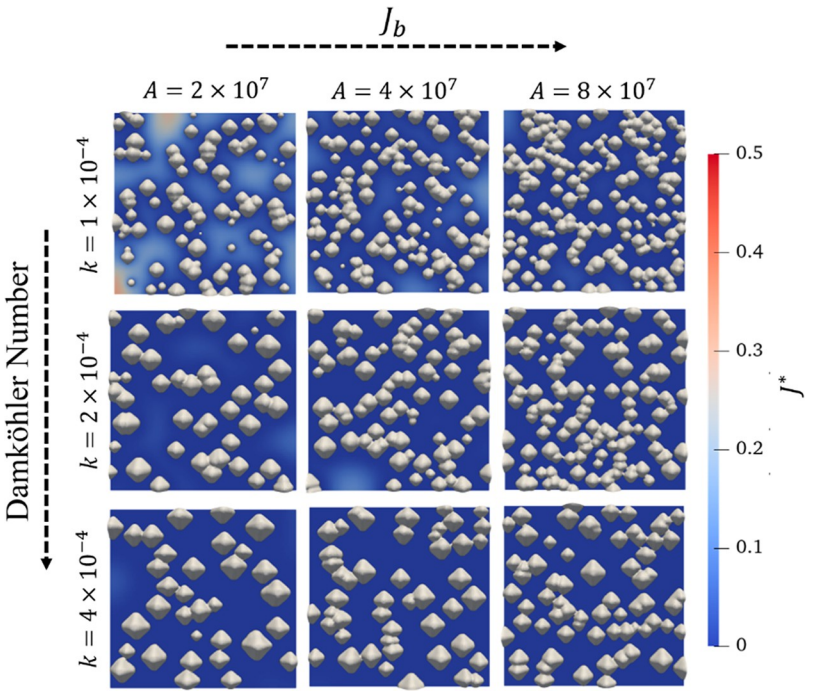

Figure 6. Distribution of scaled nucleation rate, J^*, at different Da and J_b (t = 10000 s, gray area: solid phase).

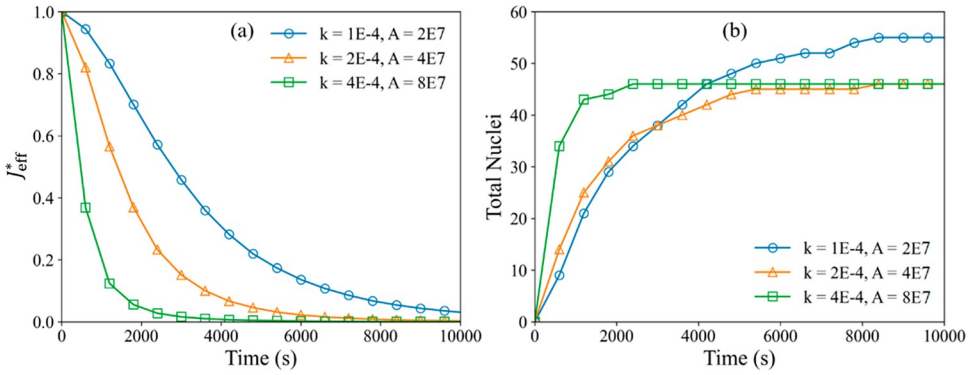

Figure 7. (a) Effective nucleation rate J^*_{eff} as a function of time for different inputted k and A, while maintaining α = 3.8. (b) Total nuclei formed on the substrate as a function of time for different inputs of k and A, while maintaining α = 3.8.

function of time, faster at higher A. In contrast to the Da number study, this phenomenon can be simply explained by faster generation of nuclei on the substrate (Figure 5b). It is interesting to note that an increase in nucleation rate leads to higher ultimate nucleation density (plateau in Figure 5b), an opposite result from the increase in the reaction rate (Da) (Figure 3b).

In Figure 6 we summarize the effect of nucleation and reaction rates. We demonstrate snapshots of precipitate and distribution of effective nucleation rate on the substrate at 10000 s for different Da and initial nucleation rate, J_b. It is found that, as the Da number increases, the total number of nuclei decreases, while the average size of the crystals increases. To the contrary, as the bulk/initial nucleation rate J_b increases, the total number of nuclei increases, while the average size of the crystals decreases. Another interesting observation is the effect of the proximity of growing crystals, which further reduces the local nucleation rate, J^*, in the vicinity of a cluster of growing crystals. More specifically, a substrate surface far away from any existing crystals has a higher chance of nucleating a new crystal. This result indicates that the nucleation rates in a multicrystal system measured from experiments could be affected by the crystal growth rate due to the suppression in depletion zones (shown by red circles in Figure 4) surrounding growing nuclei. Depletion zones are larger at higher Damköhler numbers.

4.3. Controls on the Nucleation Process. As the previous sections have shown, during mineral growth, all three processes, crystal nucleation, crystal growth, and transport of reactive species, are interconnected. To address this challenge, we explore the interplay of mechanisms (nucleation rate versus growth of existing crystals) that control the governing equations describing these processes.

Thus, we propose a dimensionless number α, described in Section 2, which represents the ratio between the growth rate and the heterogeneous nucleation rate (eq 6). We adopt this simple form as illustrative. Following this, we change the prefactors A and k simultaneously to maintain α as constant in the bulk solution environment. In such way, we expected to observe universality during the entire precipitation process. We

https://doi.org/10.1021/acsearthspacechem.1c00376
ACS Earth Space Chem. 2022, 6, 1655−1665

studied this relation by changing the reaction and nucleation rates simultaneously while maintaining the α constant at α = 3.8.

Contrary to our expectations, the simulations revealed that scaling the reaction and nucleation rates at the same time results in a different precipitation process (Figure 7). For instance, when $k = 4 \times 10^{-4}$ m/s and $A = 8 \times 10^{7}$ nuclei/m^2/s, formation of the crystals in the system was much faster compared to the other two cases (Figure 7b). Also, the effective nucleation rate dropped more rapidly (Figure 7a). Hence, by only controlling the nondimensional number α, it is not sufficient to control the nuclei density during the precipitation process.

To explain this behavior, one needs to take into account transport of reactive species. By changing nucleation rate and reaction rate to keep α constant, we change the Da number. Therefore, in order to keep both dimensionless parameters constant, the diffusion coefficient needs to be scaled as well. In actuality, diffusion coefficients only will change if something about the system changes, for instance, by increasing/reducing ion concentration in the solution (Onsager interaction between neighboring ion clouds), temperature, or addition of a different solvent, for example, ethanol. Here, however, we perform these as an experiment to understand the role that transport of ions plays in the precipitation process. Table 1 shows four different simulation scenarios with varying input parameters while maintaining both Da and α constant.

Table 1. Input Parameters for Different Simulation Scenarios

simulation scenarios	k (m/s)	D (m^2/s)	A (nuclei/m^2/s)	Da	α
1	2×10^{-4}	2×10^{-9}	4×10^{7}	5	3.8
2	3×10^{-4}	3×10^{-9}	6×10^{7}	5	3.8
3	4×10^{-4}	4×10^{-9}	8×10^{7}	5	3.8
4	5×10^{-4}	5×10^{-9}	1×10^{8}	5	3.8

Figure 8 shows the effective J^*_{eff} and total nuclei number as a function of dimensionless time ($t^* = tD/H^2$). It shows that both properties J^*_{eff} (Figure 8a) and total number of nuclei (Figure 8b) for all four cases become similar. Moreover, the distribution of J^* and solid phase formed on substrate at t^* = 4000 (Figure 9) demonstrates that all four scenarios are alike to each other: total number of nuclei, crystal size, and nucleation rate distribution on substrate, etc. We can conclude from this exercise that, by controlling both the Da and α, the nucleation process demonstrates universal behavior. This indicates that it is possible to regulate the precipitation process within a system by manipulating one or both of these terms. For instance, Yuan et al.[28] showed that strontium simultaneously increases nucleation rate and decreases growth rate, and Jones et al.[39] used methanol to enhance barite nucleation by reducing the surface tension, hence increasing the diffusion rate. A possibility to change the rate of transport is by increasing the rate of advection (i.e., fluid flow velocity in an experiment) or turbulence of the fluid flow, which might reduce the size of the diffusive boundary layer effectively simulated here,[40] or perhaps changing the substrate topography to something rougher than the perfect planar substrate used here to improve access to well-mixed fluid. Moreover, it is not clear how the nuclei themselves will change the flow patterns of the solution within a real system. Thus, since all three kinetic phenomena (transport, reaction, and nucleation rates) are interconnected, the predictive capability for how a given change to any or all of the rates translates to a change in the effective nucleation rate will need verification.

4.4. Effect of Bulk Solute Concentration and Comparison to Experiments. Here, we demonstrate how the concentration of the bulk solution affects the nucleation process to help guide future experiment design. We emphasize that in the current study, we consider only the interplay between nucleation, reaction, and diffusive transport. Therefore, a different behavior is expected if the convective transport is included. As the bulk solute concentration increases, the system behavior transits from growth dominated regime to the nucleation dominated regime (α decreases), as Figure 10c shows. Fixed parameters in this case are the diffusion coefficient $D = 1 \times 10^{-9}$ m^2/s, solid-phase molar mass M_v = 200 g/mol, surface energy γ = 33 mJ/m^2, and molar volume $V_{mol} = 5 \times 10^{-5}$ m^3/mol. The reaction rate constant $k = 1 \times 10^{-4}$ m/s and nucleation rate prefactor $A = 8 \times 10^{7}$ nuclei/m^2/s, while the SI was varied between 1.5 and 2.5.

Figure 10a,b shows time dependence of J^*_{eff} and total nuclei formed on the substrate for different SI of bulk solution. Although effective nucleation rate drops significantly faster at higher SI (Figure 10a), the total number of nuclei reaches a higher limit at higher SI, meaning that eventually there will be higher nuclei density on a substrate. Such an outcome corresponds to transition from growth to nucleation-

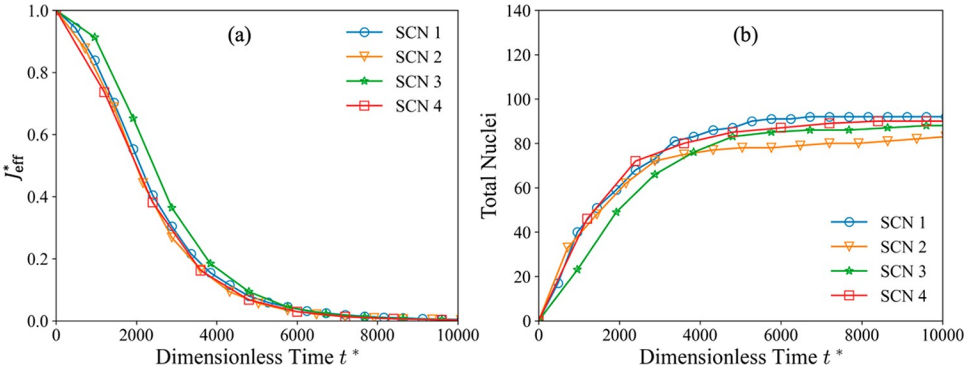

Figure 8. (a) Effective nucleation rate, J^*_{eff}, as a function of time for different scenarios (SCN) from Table 1. (b) Total nuclei formed on substrate as a function of time for different scenarios (SCN) from Table 1. For reference, in SCN 1 (smallest diffusion rate value) dimensionless time of t^* = 10000 corresponds to t = 12500 s.

https://doi.org/10.1021/acsearthspacechem.1c00376
ACS Earth Space Chem. 2022, 6, 1655−1665

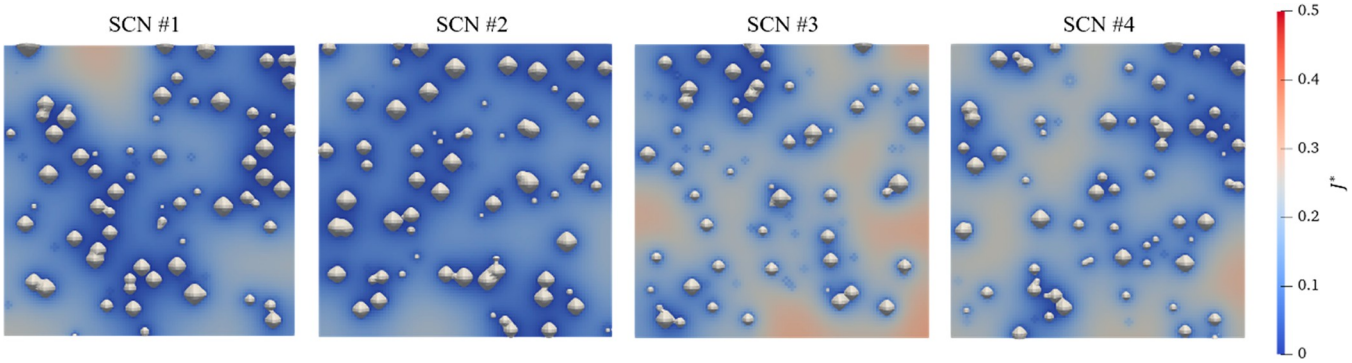

Figure 9. Scaled nucleation rate, J^*, contour maps for different scenarios at $t^* = 4000$ (gray area: solid phase).

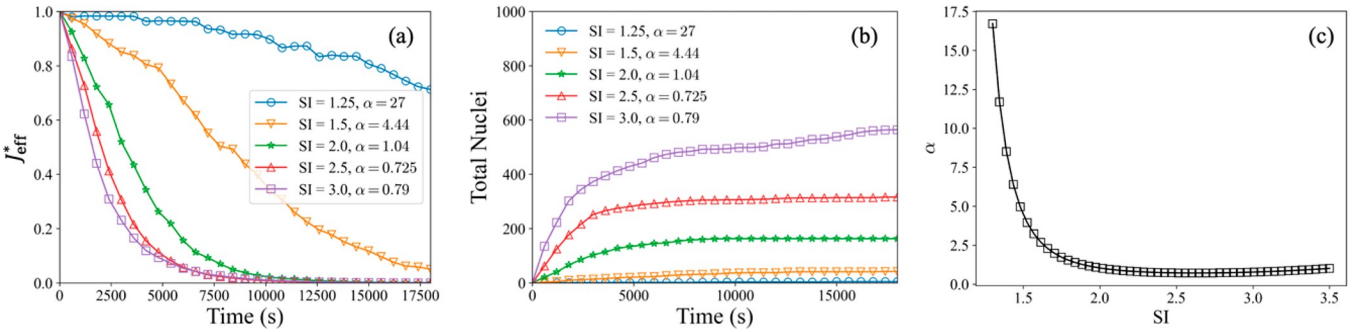

Figure 10. (a) Effective nucleation rate, J^*_{eff}, as a function of time for different bulk solution concentration. (b) Total nuclei formed on substrate as a function of time for different bulk solution concentration. (c) Dimensionless number α as a function of SI.

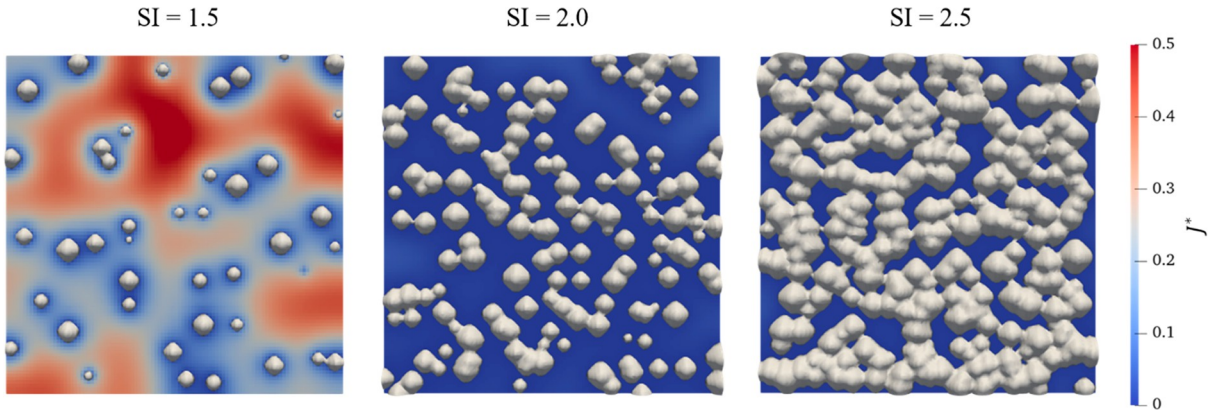

Figure 11. Scaled nucleation rate, J^*, contour maps for different bulk solute concentrations at 15000 s (gray area: solid phase).

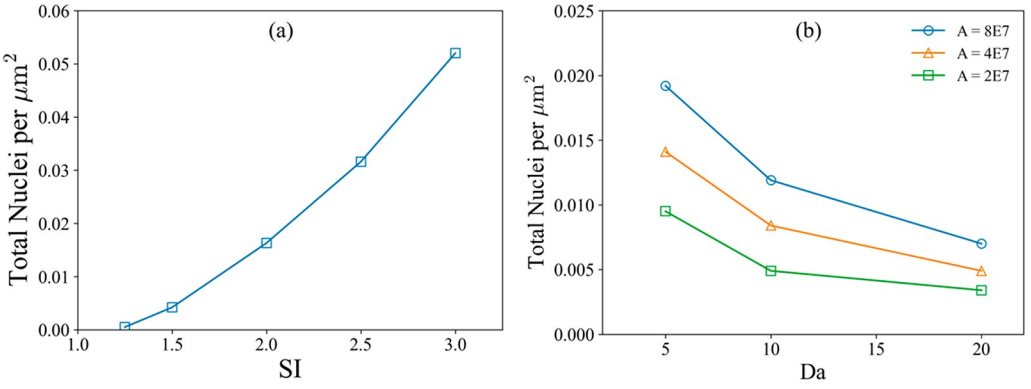

Figure 12. (a) Total nuclei per area on substrate for (a) different SI and (b) as a function of *Da* number and nucleation prefactor *A*.

https://doi.org/10.1021/acsearthspacechem.1c00376
ACS Earth Space Chem. 2022, 6, 1655−1665

dominated regime at high SI (see Figure 10c). In Figure 11 snapshots of the substrate at different SI values are demonstrated. The snapshots are taken at the same simulation time for comparison. The color map shows the local distribution of scaled J^* and solid precipitate on the substrate. It is interesting to note that although at SI = 2.0, there are still open areas on the substrate similar to SI = 1.5, effectively, the nucleation is not happening.

Since the total number of nuclei plateaus, or saturates, once the effective nucleation rate drops significantly, we can estimate the nucleation densities for different SI. Figure 12a shows the total nuclei per area increases with increasing SI. This result is unexpected since Figure 10c demonstrates that α almost does not change at SI > 2.0. We suggest that observed increases in nucleation density with increasing SI at SI > 2.0 (e.g., ref 28) is a result of the effects of convective transport which was discussed in section above.

Another interesting observation is that at higher Da (Da = 20), the nucleation densities depend less on nucleation rate (prefactor A) than at lower Da (Figure 12b). This result indicates that the impact of the nucleation rate becomes less important for the higher reaction rate cases. Extremely high reaction rates can potentially consume most of the available reactant near the substrate and cause the concentration to drop below the saturation concentration for crystal nucleation, creating a self-limiting condition for nucleation rate.

It is important to compare the qualitative results of this model, where a reduction in the effective nucleation rate as a function of time is observed, to experimental observations. A recent measurement on a similar smooth substrate, but using flowing solution passing through a small capillary tube (~100 μm in diameter), determined nucleation rates through fast synchrotron-based X-ray nanotomography with a 30 nm resolution.[28] There, no plateau or reduction of the nucleation rate is observed, and the time series is remarkably linear. Although the Da values were small (~0.01) in these experiments, the absence of plateau is possibly related by dominant convective transport due to the flow through the capillary. The competition between growth and transport is more significant at higher saturation states or during dissolution−reprecipitation reactions, in which the local concentration can be much higher than in bulk solutions.[41] Under these conditions, higher Da values are expected, and the simulation results demonstrated in this work will be directly applicable.

On the other hand, there have also been multiple measurements using batch reactor type setups without flowing solution, where a supersaturated solution is created within a reactor and subsequently nucleated particle volumes are observed using, for example, grazing incidence small-angle X-ray scattering.[33,42,43] These frequently show plateauing of the measured total particle volumes scattering the X-ray beam, consistent with the reductions shown here. Thus, these results are relevant to situations where there is a substantial diffusion control on nucleation and growth. Porous media is an example where this type of environment might be present, in that there is a continuum of flow rates within different distributions of pores.

5. CONCLUSION

In this study, we incorporated heterogeneous nucleation, which follows classical nucleation theory, into a micro-continuum reactive transport model based on the DBS approach. The implementation of nucleation is based on a stochastic process.

It was shown that a zoning effect in the vicinity of crystals, where a diffusion gradient created by reactant consumption during crystal growth, suppressed subsequent nucleation on the substrate and led to plateaued or saturated nuclei densities. In general, it was found that the nucleation of new crystals was always suppressed by the growth of nearby existing crystals and the magnitude of the suppression is higher for higher Da numbers. This suggests that nucleation rates measured in experiments could potentially be affected by this phenomenon, especially where growth rates are higher. To better understand the processes affecting the nucleation rate, a nondimensional number α was introduced to represent the relation between interfacial reaction rate and surface nucleation rate. To regulate the effective nucleation process, it was found that not only should α be controlled but also the Da number plays a role in determining the extent of the zoning effect. By fixing α and Da simultaneously, the modeled system demonstrates universality. This result is important for interpretation of experimental nucleation rate findings. Transport, reaction, and nucleation parameters should be considered simultaneously to eliminate ambiguity in interpretation of fitting parameters. Finally, the study of the effects of bulk solute concentration (saturation index) on the total nuclei density on the substrate have supported importance of reported universality for experimental findings, in which SI is a common parameter. It was shown that, with increasing of SI, α decreases rapidly at $1 \lesssim \mathrm{SI} \lesssim 2$ and stays constant at $\mathrm{SI} \gtrsim 2.0$; however, nuclei density continues to increase over the whole range of SI.

In summary, this study used the DBS model to investigate the underlying mechanisms that may affect the nucleation process. The versatility of the DBS model coupled with classical nucleation theory opens a way for broader applications where the nucleation coexists with surface reaction or a phase transformation. However, further detailed studies are still needed to understand the effect of different flow conditions, complex geometries, as well as multiple surface reactions, more realistic growth rate expressions, and wider ranges of heterogeneous nucleation rates, during the precipitation process. The results of this study are expected to shed light on the mechanism of crystal nucleation on a solid boundary and help the future design of related experiments.

AUTHOR INFORMATION

Corresponding Authors

Fengchang Yang − *Chemical Sciences Division, Oak Ridge National Laboratory, Oak Ridge, Tennessee 37831, United States;* Present Address: Institute of Mechanics, Chinese Academy of Sciences, 15 Beisihuanxi Road, Beijing 100190, China; Email: yangfengchang@imech.ac.cn

Vitalii Starchenko − *Chemical Sciences Division, Oak Ridge National Laboratory, Oak Ridge, Tennessee 37831, United States;* orcid.org/0000-0003-2313-7379; Email: starchenkov@ornl.gov

Authors

Ke Yuan − *Chemical Sciences Division, Oak Ridge National Laboratory, Oak Ridge, Tennessee 37831, United States;* orcid.org/0000-0003-0565-0929

Andrew G. Stack − *Chemical Sciences Division, Oak Ridge National Laboratory, Oak Ridge, Tennessee 37831, United States;* orcid.org/0000-0003-4355-3679

https://doi.org/10.1021/acsearthspacechem.1c00376
ACS Earth Space Chem. 2022, 6, 1655−1665

Complete contact information is available at:
https://pubs.acs.org/10.1021/acsearthspacechem.1c00376

Notes

The authors declare no competing financial interest.

■ ACKNOWLEDGMENTS

This material is based upon work supported by the U.S. Department of Energy, Office of Science, Office of Basic Energy Sciences, Chemical Sciences, Geosciences, and Biosciences Division. This research used resources of the Compute and Data Environment for Science (CADES) at the Oak Ridge National Laboratory, which is supported by the Office of Science of the U.S. Department of Energy under contract no. DE-AC05-00OR22725 as well as the National Energy Research Scientific Computing Center (NERSC) clusters, a U.S. Department of Energy Office of Science User Facility operated under contract no. DE-AC02-05CH11231.

■ REFERENCES

(1) Weiner, S.; Addadi, L. Crystallization Pathways in Biomineralization. *Annu. Rev. Mater. Res.* **2011**, *41*, 21−40.
(2) De Yoreo, J. J.; Vekilov, P. G. Principles of Crystal Nucleation and Growth. *Rev. Mineral. Geochemistry* **2003**, *54* (1), 57.
(3) Koop, T.; Luo, B.; Tsias, A.; Peter, T. Water Activity as the Determinant for Homogeneous Ice Nucleation in Aqueous Solutions. *Nature* **2000**, *406* (6796), 611−614.
(4) Olafson, K. N.; Ketchum, M. A.; Rimer, J. D.; Vekilov, P. G. Mechanisms of Hematin Crystallization and Inhibition by the Antimalarial Drug Chloroquine. *Proc. Natl. Acad. Sci. U. S. A.* **2015**, *112* (16), 4946−4951.
(5) Crabtree, M.; Eslinger, D.; Fletcher, P.; Miller, M.; Johnson, A. Fighting Scale: Removal and Prevention. *Oilfield Rev.* **1999**, *11* (03), 30−45.
(6) Wigg, H.; Fletcher, M. Establishing the True Cost of Downhole Scale Control. Proceedings from the *International Conference on Solving Oilfield Scaling, Aberdeen, Scotland,* Aberdeen, Scotland, November 20−21, 1995; SPE: London, 1995.
(7) Li, H.; Kawajiri, Y.; Grover, M. A.; Rousseau, R. W. Modeling of Nucleation and Growth Kinetics for Unseeded Batch Cooling Crystallization. *Ind. Eng. Chem. Res.* **2017**, *56* (14), 4060−4073.
(8) De Yoreo, J. J.; Gilbert, P. U. P. A.; Sommerdijk, N. A. J. M.; Penn, R. L.; Whitelam, S.; Joester, D.; Zhang, H.; Rimer, J. D.; Navrotsky, A.; Banfield, J. F.; Wallace, A. F.; Michel, F. M.; Meldrum, F. C.; Cölfen, H.; Dove, P. M. Crystallization by Particle Attachment in Synthetic, Biogenic, and Geologic Environments. *Science* **2015**, *349* (6247), aaa6760.
(9) Dashtian, H.; Wang, H.; Sahimi, M. Nucleation of Salt Crystals in Clay Minerals: Molecular Dynamics Simulation. *J. Phys. Chem. Lett.* **2017**, *8* (14), 3166−3172.
(10) Lutsko, J. F. How Crystals Form: A Theory of Nucleation Pathways. *Sci. Adv.* **2019**, *5* (4), No. eaav7399.
(11) Molins, S.; Soulaine, C.; Prasianakis, N. I.; Abbasi, A.; Poncet, P.; Ladd, A. J. C.; Starchenko, V.; Roman, S.; Trebotich, D.; Tchelepi, H. A.; Steefel, C. I. Simulation of Mineral Dissolution at the Pore Scale with Evolving Fluid-Solid Interfaces: Review of Approaches and Benchmark Problem Set. *Comput. Geosci.* **2021**, *25* (4), 1285−1318.
(12) Li, X.; Huang, H.; Meakin, P. Level Set Simulation of Coupled Advection-Diffusion and Pore Structure Evolution Due to Mineral Precipitation in Porous Media. *Water Resour. Res.* **2008**, *44* (12), 6742.
(13) Xu, Z.; Meakin, P. Phase-Field Modeling of Two-Dimensional Solute Precipitation/Dissolution: Solid Fingers and Diffusion-Limited Precipitation. *J. Chem. Phys.* **2011**, *134* (4), 044137.
(14) Xu, Z.; Meakin, P. Phase-Field Modeling of Solute Precipitation and Dissolution. *J. Chem. Phys.* **2008**, *129* (1), 014705.
(15) Soulaine, C.; Roman, S.; Kovscek, A.; Tchelepi, H. A. Mineral Dissolution and Wormholing from a Pore-Scale Perspective. *J. Fluid Mech.* **2017**, *827*, 457−483.
(16) Soulaine, C.; Creux, P.; Tchelepi, H. A. Micro-Continuum Framework for Pore-Scale Multiphase Fluid Transport in Shale Formations. *Transp. Porous Media* **2019**, *127* (1), 85−112.
(17) Kang, Q.; Lichtner, P. C.; Zhang, D. An Improved Lattice Boltzmann Model for Multicomponent Reactive Transport in Porous Media at the Pore Scale. *Water Resour. Res.* **2007**, *43* (12), 1−12.
(18) Jones, T. A.; Detwiler, R. L. Mineral Precipitation in Fractures: Using the Level-Set Method to Quantify the Role of Mineral Heterogeneity on Transport Properties. *Water Resour. Res.* **2019**, *55* (5), 4186−4206.
(19) Tartakovsky, A. M.; Meakin, P.; Scheibe, T. D.; Eichler West, R. M. Simulations of Reactive Transport and Precipitation with Smoothed Particle Hydrodynamics. *J. Comput. Phys.* **2007**, *222* (2), 654−672.
(20) Tartakovsky, A. M.; Meakin, P.; Scheibe, T. D.; Wood, B. D. A Smoothed Particle Hydrodynamics Model for Reactive Transport and Mineral Precipitation in Porous and Fractured Porous Media. *Water Resour. Res.* **2007**, *43* (5), 4770 DOI: 10.1029/2005WR004770.
(21) Kang, Q.; Lichtner, P. C.; Zhang, D. Lattice Boltzmann Pore-Scale Model for Multicomponent Reactive Transport in Porous Media. *J. Geophys. Res. Solid Earth* **2006**, *111* (B5), 203.
(22) Kang, Q.; Lichtner, P. C.; Janecky, D. R. Lattice Boltzmann Method for Reacting Flows in Porous Media. *Adv. Appl. Math. Mech.* **2019**, *2* (5), 545−563.
(23) Yang, F.; Stack, A. G.; Starchenko, V. Micro-Continuum Approach for Mineral Precipitation. *Sci. Rep.* **2021**, *11* (1), 3495.
(24) Prasianakis, N. I.; Curti, E.; Kosakowski, G.; Poonoosamy, J.; Churakov, S. V. Deciphering Pore-Level Precipitation Mechanisms. *Sci. Rep.* **2017**, *7* (1), 13765.
(25) Starchenko, V. Pore-Scale Modeling of Mineral Growth and Nucleation in Reactive Flow. *Front. Water* **2022**, *3*, 190.
(26) Deng, H.; Tournassat, C.; Molins, S.; Claret, F.; Steefel, C. I. A Pore-Scale Investigation of Mineral Precipitation Driven Diffusivity Change at the Column-Scale. *Water Resour. Res.* **2021**, *57* (5), No. e2020WR028483.
(27) Deng, H.; Poonoosamy, J.; Molins, S. A Reactive Transport Modeling Perspective on the Dynamics of Interface-Coupled Dissolution-Precipitation. *Appl. Geochem.* **2022**, *137*, 105207.
(28) Yuan, K.; Starchenko, V.; Rampal, N.; Yang, F.; Yang, X.; Xiao, X.; Lee, W.-K. K.; Stack, A. G. G. Opposing Effects of Impurity Ion Sr 2+ on the Heterogeneous Nucleation and Growth of Barite (BaSO 4). *Cryst. Growth Des.* **2021**, *21* (10), 5828−5839.
(29) Steefel, C. I.; Yang, L. Secondary Magnesite Formation from Forsterite under CO2 Sequestration Conditions via Coupled Heterogeneous Nucleation and Crystal Growth. *Geochim. Cosmochim. Acta* **2021**, *311*, 29−42.
(30) Fazeli, H.; Masoudi, M.; Patel, R. A.; Aagaard, P.; Hellevang, H. Pore-Scale Modeling of Nucleation and Growth in Porous Media. *ACS Earth Sp. Chem.* **2020**, *4* (2), 249−260.
(31) Khadra, K.; Angot, P.; Parneix, S.; Caltagirone, J.-P. Fictitious Domain Approach for Numerical Modelling of Navier-Stokes Equations. *Int. J. Numer. Methods Fluids* **2000**, *34* (8), 651−684.
(32) Mullin, J. W. *Crystallization*; Elsevier: London, 2001.

(33) Fernandez-Martinez, A.; Hu, Y.; Lee, B.; Jun, Y.-S.; Waychunas, G. A. In Situ Determination of Interfacial Energies between Heterogeneously Nucleated CaCO3 and Quartz Substrates: Thermodynamics of CO2 mineral Trapping. *Environ. Sci. Technol.* **2013**, *47* (1), 102−109.
(34) Godinho, J. R. A.; Stack, A. G. Growth Kinetics and Morphology of Barite Crystals Derived from Face-Specific Growth Rates. *Cryst. Growth Des.* **2015**, *15* (5), 2064−2071.
(35) Parkhurst, D. L.; Appelo, C. A. J. Description of Input and Examples for PHREEQC Version 3 — A Computer Program for Speciation, Batch-Reaction, One-Dimensional Transport, and Inverse Geochemical Calculations. *U.S. Geological Survey Techniques and Methods*; USGS: Reston, VA, 2013; book 6, chapter A43.
(36) Jasak, H.; Jemcov, A.; Tukovic, Z. OpenFOAM : A C + + Library for Complex Physics Simulations. Proceedings from the *International Workshop on Coupled Methods in Numerical Dynamics*, Dubrovnik, Croatia, September 19−21, 2007; Inter-University Centre Dubrovnik: Dubrovnik, Croatia, 2007; Vol. *1000*, pp 1−20.
(37) Wang, H. W.; Yuan, K.; Rampal, N.; Stack, A. G. Solution and Interface Structure and Dynamics in Geochemistry: Gateway to Link Elementary Processes to Mineral Nucleation and Growth. *Cryst. Growth Des.* **2022**, *22* (1), 853−870.
(38) Zhen-Wu, B. Y.; Dideriksen, K.; Olsson, J.; Raahauge, P. J.; Stipp, S. L. S.; Oelkers, E. H. Experimental Determination of Barite Dissolution and Precipitation Rates as a Function of Temperature and Aqueous Fluid Composition. *Geochim. Cosmochim. Acta* **2016**, *194*, 193−210.
(39) Jones, F.; Piana, S.; Gale, J. D. Understanding the Kinetics of Barium Sulfate Precipitation from Water and Water-Methanol Solutions. *Cryst. Growth Des.* **2008**, *8* (3), 817−822.
(40) Molins, S.; Trebotich, D.; Miller, G. H.; Steefel, C. I. Mineralogical and Transport Controls on the Evolution of Porous Media Texture Using Direct Numerical Simulation. *Water Resour. Res.* **2017**, *53* (5), 3645−3661.
(41) Nielsen, M. H.; Aloni, S.; De Yoreo, J. J. In Situ TEM Imaging of CaCO3 Nucleation Reveals Coexistence of Direct and Indirect Pathways. *Science (80-.).* **2014**, *345* (6201), 1158−1162.
(42) Deng, N.; Stack, A. G.; Weber, J.; Cao, B.; De Yoreo, J. J.; Hu, Y. Organic-Mineral Interfacial Chemistry Drives Heterogeneous Nucleation of Sr-Rich (Bax, Sr1- x) SO4 from Undersaturated Solution. *Proc. Natl. Acad. Sci. U. S. A.* **2019**, *116* (27), 13221−13226.
(43) Dai, C.; Stack, A. G.; Koishi, A.; Fernandez-Martinez, A.; Lee, S. S.; Hu, Y. Heterogeneous Nucleation and Growth of Barium Sulfate at Organic-Water Interfaces: Interplay between Surface Hydrophobicity and Ba $^{2+}$ Adsorption. *Langmuir* **2016**, *32* (21), 5277−5284.

https://doi.org/10.1021/acsearthspacechem.1c00376
ACS Earth Space Chem. 2022, 6, 1655−1665